Bioinspired sweat-resistant wearable triboelectric nanogenerator for movement monitoring during exercise

Li, Wenjian; Lu, Ewan; Kottapalli, Ajay Giri Prakash; Pei, Yutao T.

Published in:
Nano energy

DOI:
10.1016/j.nanoen.2022.107018

Publication date:
2022

Nano Energy 95 (2022) 107018

Contents lists available at ScienceDirect

Nano Energy

journal homepage: www.elsevier.com/locate/nanoen

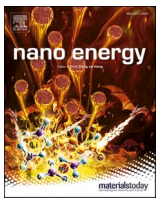

Bioinspired sweat-resistant wearable triboelectric nanogenerator for movement monitoring during exercise

Wenjian Li, Liqiang Lu, Ajay Giri Prakash Kottapalli, Yutao Pei *

Department of Advanced Production Engineering, Engineering and Technology Institute Groningen, Faculty of Science and Engineering, University of Groningen, Nijenborgh 4, 9747 AG Groningen, The Netherlands

ARTICLE INFO

Keywords:
Bioinspired
Sweat-resistant
Self-cleaning
Triboelectric nanogenerator
Movement monitoring

ABSTRACT

Regular exercise plays an important role in remedying body suboptimal health status and releasing daily stress. Herein, we proposed a bioinspired sweat-resistant wearable triboelectric nanogenearator (BSRW-TENG) for movement monitoring during exercise. The BSRW-TENG consists of two superhydrophobic and self-cleaning triboelectric layers (elastic resin and polydimethylsiloxane (PDMS)), which featured the hierarchical micro/nanostructures replicated from lotus leaf. The bioinspired micro/nanostructures not only realized a 2-fold output increase of the BSRW-TENG, but also offered the BSRW-TENG with excellent contamination and humidity resistant properties that constitute the sweat-resistance. After saline (0.9%) dripped on and evaporated, the output of the BSRW-TENG remained the same while that of the flat-TENG decreased by 41% due to salt contamination on the triboelectric surfaces. Besides, the BSRW-TENG demonstrated excellent humidity-resistance with only 11% output reduction as the relative humidity increased from 10% to 80%, while the flat-TENG decreased by 54%. The sweat-resistant ability was further verified under extreme harsh conditions including complete surface contamination and ultra-humid water spraying. Finally, various exercise movements including dumbbell biceps curl, leg curl and running were successfully monitored by the BSRW-TENG with stable performance before and after sweating. The proposed BSRW-TENG has huge potential in low-cost personal exercise monitoring and athletes' training analysis.

1. Introduction

Body suboptimal health is gaining increasing attention as a public health issue since it is troubling most of the people. According to the Global Burden of Disease Study 2013, 75% of the world's population are in suboptimal health status (SHS), including aches, sleep disorders, chronic fatigue, poor mood, depression and so on [1]. In order to get rid of the SHS, more and more people choose to conduct regular exercise and fitness. The popularity of exercise and fitness is also attributed to its benefits for relieving huge work stress and reshaping physical beauty. However, incorrect exercise movement can not only fail to improve the physical health status, but can make the SHS worse and even get injured [2,3]. Exercise movement monitoring and analysis can effectively regulate incorrect movements and thus effectively easing the SHS body. Currently, movement monitoring mainly relies on manual guidance accomplished through trained human coaches, which could be an expensive deal. Commercial sports bracelets and watches can only provide information about heart rate, exercise time and distance, but are unable to monitor a specific exercise and fitness movement. As a result, developing low-cost monitoring devices that can monitor and analyze movement amplitude, speed, frequency and even its dynamic process has great potential in improving people's health status. Moreover, dynamic analysis of athletes' exercise movements can enable them to discover tiny imperfections in their training and thus improve their performances.

Recent successes in the development of flexible and wearable electronics [4] that can be attached or worn conformally onto the human body demonstrate huge prospects in physiological condition monitoring and personalized healthcare, such as sweat analysis [5,6], pulse monitoring [7,8], drug release [9,10] and so on. Meanwhile, achieving ultra-low power consumption and even self-powered wearable devices [11] is always coveted for the reasons of stable power supply and use of convenience. The triboelectric nanogenerators (TENGs) [12], which are based on the coupling effect of contact electrification and electrostatic induction, feature a unique advantage in self-powered sensing and self-powered systems [13]. Equipped with merits of wide range of

* Corresponding author.
E-mail address: y.pei@rug.nl (Y. Pei).

https://doi.org/10.1016/j.nanoen.2022.107018
Received 18 December 2021; Received in revised form 27 January 2022; Accepted 1 February 2022
Available online 3 February 2022

material choice, simple structure, high output and so on, TENGs are widely applied in designing and developing flexible and wearable devices [14,15], especially triboelectric electronic skins [16] and wearable energy harvesters [17]. However, the output performance and stability of TENGs can be easily affected and even dramatically degraded due to triboelectric surface contamination [18] and high environmental humidity [19]. Especially for TENG-based wearable devices, contamination, high humidity and even water droplets are unavoidable issues due to inevitable sweat secretion of the human body, especially during exercise. If the body sweats in the vicinity of the TENG, the regional humidity would increase significantly and sweat may even flow and penetrate into the triboelectric interface, thus affecting the performance of the TENG temporarily. Moreover, the penetrated sweat can leave non-removable contaminations composed of various salts in the sweat on triboelectric surfaces after its evaporation, which can cause unrecoverable and permanent performance degradation of the TENG. Encapsulating the TENG using water-resistant films is a widely applied way to protect the TENG from environmental influence, but it would affect the output performance and wearing conformality of the TENG. It was reported that the output of the TENG dramatically decreased from 200 V to 70 V after encapsulation [20] and possible tiny leakage would cause serious damage to the device [21]. In a pursuit to realize stable wearable TENGs, some humidity-resistant TENGs [22–24] were successfully developed in the past for wearable sensors and energy harvesters that can resist high humidity. However, there are scarce researches on sweat-resistant wearable TENGs that can not only stand sweat-caused humidity changes but more importantly also resist the sweat-caused salt contamination.

Here in this work, we proposed a bioinspired sweat-resistant wearable triboelectric nanogenearator (BSRW-TENG) for movement monitoring during exercise and fitness. The BSRW-TENG consists of two bioinspired superhydrophobic and self-cleaning triboelectric layers (elastic resin and polydimethylsiloxane (PDMS)), which featured the hierarchical micro/nanostructures replicated from lotus leaf. The micro/nanostructures on the resin and PDMS triboelectric surfaces benefited the electrical performance enhancement of the BSRW-TENG, which demonstrated a 2-fold increase compared to the TENG with flat surfaces (flat-TENG). Moreover, the BSRW-TENG was endowed with contamination-resistant and humidity-resistant properties that finally contributed to the sweat-resistance. The output of the BSRW-TENG remained the same after saline (0.9%) dripped and evaporated on the triboelectric surfaces, while that of the flat-TENG decreased by 41% due to salt contamination left. When the relative humidity increased from 10% to 80%, the output of the BSRW-TENG and flat-TENG demonstrated a 11% and 54% reduction, respectively, reviewing the excellent humidity-resistant ability. The remarkable sweat-resistance of the BSRW-TENG was further verified through its enhanced output recovery after complete surface contamination, less degradation and faster

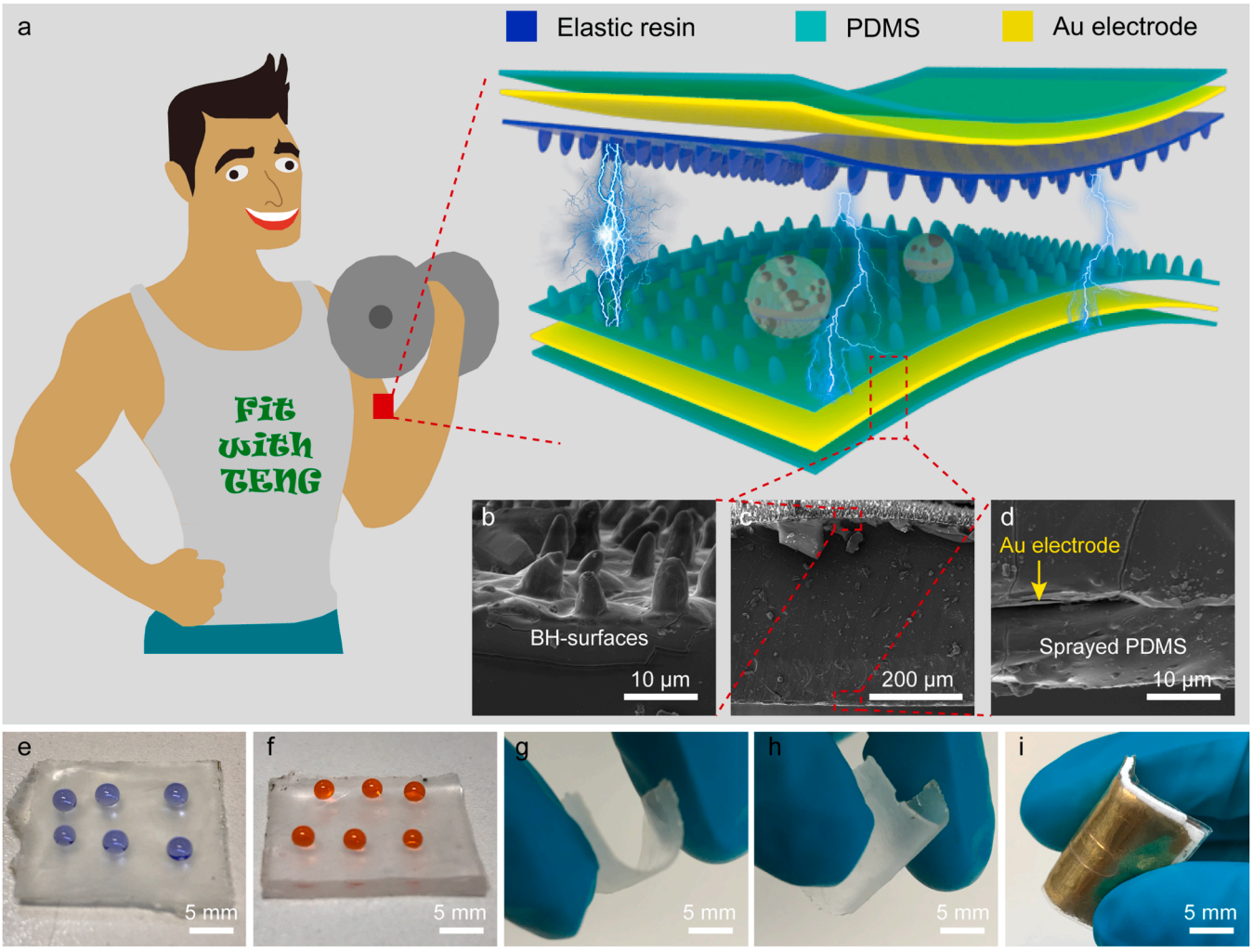

Fig. 1. (a) Schematic structure of the BSRW-TENG. (b, c and d) SEM images of the interlayer structure between the triboelectric layer, the electrode and the protection layer. (e) The superhydrophobic property of the BH-resin. (f) The superhydrophobic property of the BH-PDMS. (g) Photo of the BH-resin triboelectric layer. (h) Photo of the BH-PDMS triboelectric layer. (i) Photo of the fabricated BSRW-TENG.

recovery from ultra-humid water jet spraying. Finally, the BSRW-TENG was successfully demonstrated to monitor various exercise movements, including dumbbell biceps curl, leg curl and running, with stable and sustainable performance before and after sweating.

2. Results and discussion

The structure of the BSRW-TENG is schematically illustrated in Fig. 1**a**. The triboelectric surfaces of the BSRW-TENG consist of a bioinspired hierarchical resin (BH-resin) and a bioinspired hierarchical PDMS (BH-PDMS), which are superhydrophobic and self-cleanable with bioinspired hierarchical morphologies from the lotus leaf. A layer of Au (100 nm thick) was deposited on the backside of the BH-resin and BH-PDMS as the electrode. To protect the electrodes from corrosion due to sweat, a thin layer of PDMS (10 μm thick) was subsequently spray-coated on the Au electrodes. Fig. 1**b-d** are scanning electron microscope (SEM) images showing the interlayer structure between the triboelectric layer, the Au electrode and the spray-coated PDMS protection layer. Fig. 1**e** and **f** demonstrate the superhydrophobic property of the BH-resin and the BH-PDMS. As it can be seen from the photographs, water drops could withhold the spherical shape with high contact angles on the two bioinspired triboelectric surfaces. Fig. 1**g-h** show the photos of the BH-resin triboelectric layer, the BH-PDMS triboelectric layer and the fabricated BSRW-TENG, respectively. Fig. S1 (supporting information) shows the tensile test results of the BH-resin and the BH-PDMS, revealing excellent stretchability of the two materials.

In order to fabricate the bioinspired hierarchical micro/nanostructures on the BH-resin and the BH-PDMS triboelectric layers, a simple and cost effective soft lithography method was employed. Through soft lithographic templating, the micro/nanostructure morphology on the lotus leaf was replicated and transferred onto the curable elastic resin and PDMS, resulting in the BH-resin and BH-PDMS, respectively. The replication process of the hierarchical micro/nanostructures of the lotus leaf is illustrated in Fig. 2**a**, and the overall fabrication procedures can be seen in Fig. S2. Firstly, a piece of dried lotus leaf was conformally attached onto a 3D printed mold to serve as the original template. A photo of the dried lotus leaf is shown in Fig. S3. The surface microstructure of the dried lotus leaf features a hierarchical micro/nanostructure of microtower arrays with extensive villi on them, a complex intricate morphology that exhibits superhydrophobic and self-cleaning property with a water contact angle (WCA) of 157.9°, as shown in Fig. S4a. Secondly, uncured PDMS mixture was poured into the mold to completely cover the lotus leaf in order to realize the first replication, following which the fully cured PDMS layer was peeled off from the lotus leaf. The obtained PDMS layer was equipped with reverse micro/nanostructures from the lotus leaf (Fig. S4b) and served as a negative template for the next templating step. The second replication involved pouring the uncured resin and PDMS onto the negative templates, respectively, followed by curing and demolding. In the case of the elastic resin, in order to completely cure the material, UV curing as well as thermal curing were simultaneously required (which will be simply referred to as UV curing hereafter). In the case of the PDMS replica, a 10 nm thick Cu layer was deposited on the negative PDMS template as a sacrificial layer prior to pouring the uncured PDMS to ensure that the two PDMS layers can be successfully detached after the curing process.

The final BH-resin replica demonstrated a hierarchical micro/nanostructure morphology featuring microtower arrays with nanoscale folds and gullies on them (Fig. 2**b**). Interestingly, the UV curing time was found to be critical to the formation of the surface micro/nanostructures and the corresponding WCA of the BH-resin. Fig. 2**b** shows the SEM images of the surface micro/nanostructures and the corresponding WCAs of the BH-resin cured at different UV curing times (from 5 min to 25 min). As it can be observed, with increasing UV curing time, the complexity of the shape and the structure of the nanoscale folds and gullies on the microtowers increased but arrived at a saturation beyond a curing time of 20 min. Accordingly, the WCAs of the BH-resin also demonstrated a similar trend, increasing from 146.9° (5 min) to 157.3° (20 min), after which the superhydrophobic nature saturated.

In contrast, the surface structure of the PDMS replica showed relatively smooth microtower arrays without many nanoscale structures on them, as shown in Fig. S5. As a result, the WCA of the PDMS replica was found to be 145.6°, which is slightly lower than the requirement for superhydrophobicity (150°). To investigate the reasons for the formation of different surface morphologies on the resin and the PDMS replicas, the two polymers were separately cast and cured on flat substrates without any microstructures. The surface structures and WCAs of the flat resin and flat PDMS are shown in Fig. S6. As it can be seen, there were dense nanoscale wrinkled patterns (width ~500 nm) on the flat resin surface while in the case of PDMS the surface was quite flat. This can be explained by the mechanical deformation caused by internal stresses created during the UV and thermal curing of the high viscosity resin [25,26].

In order to realize hierarchical micro/nanostructures on the surface of the PDMS replica, flame treatment was applied to create nanostructures overlaid upon the smooth microtowers. After flame treatment, the smooth microtowers began to contain nanostructures that increased with the flame treatment time. The surface structures and the corresponding WCAs of the BH-PDMS with different flame treatment times (from 10 s to 50 s) are shown in Fig. 2**c**. The formation of the nanoscale structures on the microtowers of the PDMS surface can be attributed to two factors [27,28]. The first one is the non-uniform surface thermal stress during the reciprocating flame treatment and the second is the oxidative activation of the PDMS under high temperature flame resulting in macromolecule chains breaking into SiO_2 nanoparticles. Prior to the flame treatment, no SiO_2 nanoparticles could be observed on the microtowers. The longer the flame treatment time, the more the SiO_2 nanoparticles formed. The accumulated nanoparticles appeared to explode when the flame treatment time exceeded 30 s, forming flower petal-like nanostructures. When the flame treatment time reached 50 s, the nanoparticles on most microtowers completely exploded apart and dropped from the microtowers, slightly decreasing the WCA. As a result, the WCA firstly increased from 145.6° (0 s) to 159.4° (40 s) and then slightly decreased to 157.3° (50 s). Fig. S7 summarizes the WCA of the BH-resin and BH-PDMS as a function of the UV curing time and the flame treatment time, respectively. Finally, 20 min UV cured BH-resin and 30 s flame treated BH-PDMS were selected to construct the BSWR-TENG and for the subsequent testing for their excellent superhydrophobicity, as demonstrated in **Video S1**.

Supplementary material related to this article can be found online at doi:10.1016/j.nanoen.2022.107018.

It is well known that the superhydrophobicity is a necessary but not sufficient condition to form a self-cleaning surface, which also requires a sliding angle smaller than 10°. The sliding angles of the selected BH-resin and the BH-PDMS were tested to be about 5°. Fig. S8 shows three consecutive frames of a water drop sliding on the 5°-tilted BH-resin and BH-PDMS, respectively. The video demonstrating the full sliding motions can be seen in **Video S2**. It can be observed that the water drop rolled down faster on the BH-PDMS than on the BH-resin, since the BH-PDMS has a higher WCA caused by the ultralow surface energy SiO_2 nanoparticles.

Supplementary material related to this article can be found online at doi:10.1016/j.nanoen.2022.107018.

The working principle of the BSRW-TENG is based on the contact electrification and electrostatic induction effect, which is schematically illustrated in Fig. 3**a**. After several cycles of friction, charges begin to accumulate on the surfaces of the two triboelectric layers as a result of the contact electrification. Due to the difference in the ability to attract and lose electrons, negative charges are generated on the BH-PDMS surface while equal amounts of positive charges are generated on the BH-resin surface. When the two charged surfaces are fully in contact, as shown in the state I, there is no charge flow between the two backside electrodes due to electrostatic equilibrium. An electrostatic field is

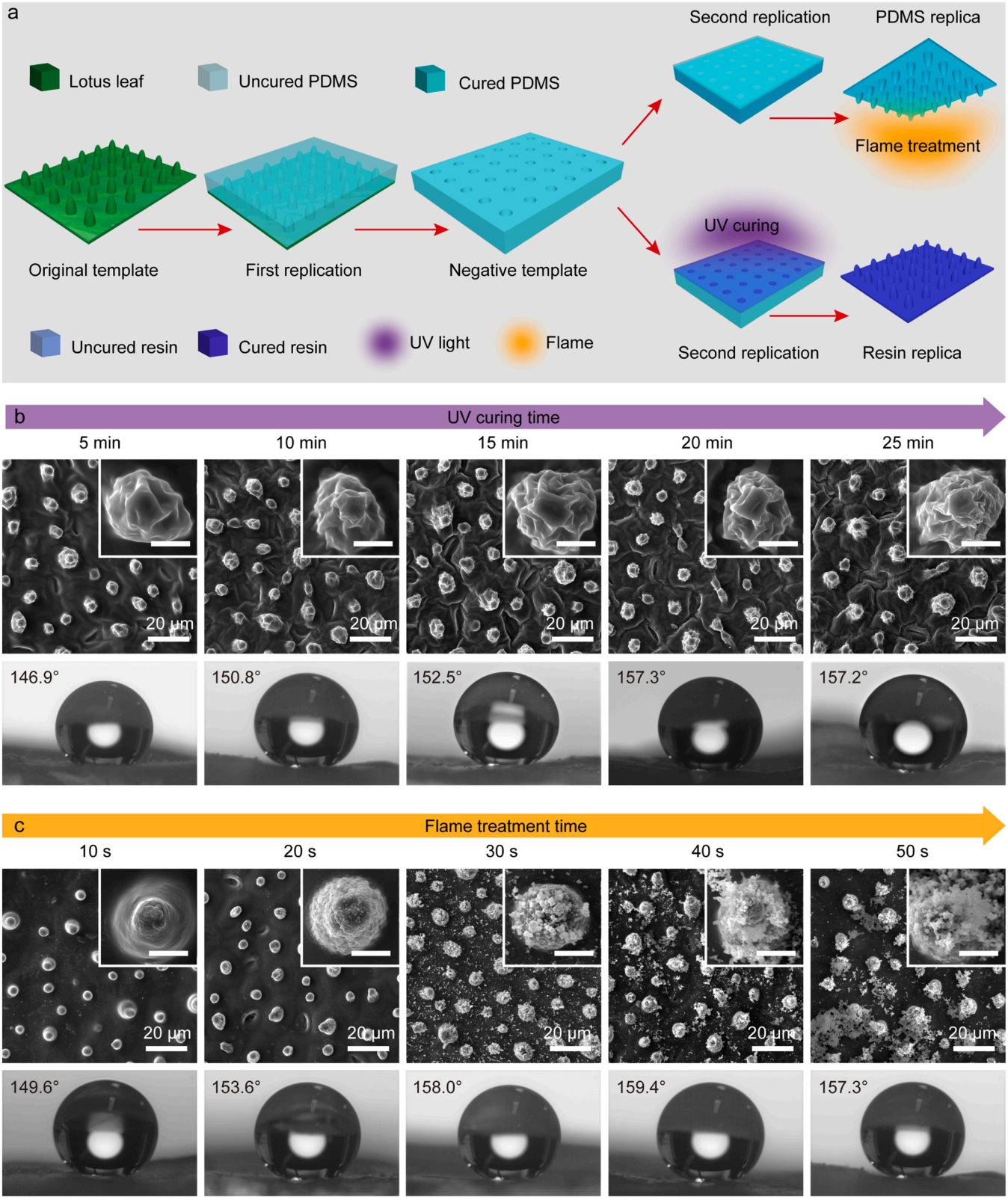

Fig. 2. (a) Replication process of the hierarchical micro/nanostructure. (b) SEM images (top) and WCA measurements (bottom) of the BH-resin with UV curing time of 5–25 min (scale bar of the insets: 5 μm). (c) SEM images (top) and WCA measurements (bottom) of the BH-PDMS with flame treatment time of 10–50 s (scale bar of the insets: 5 μm).

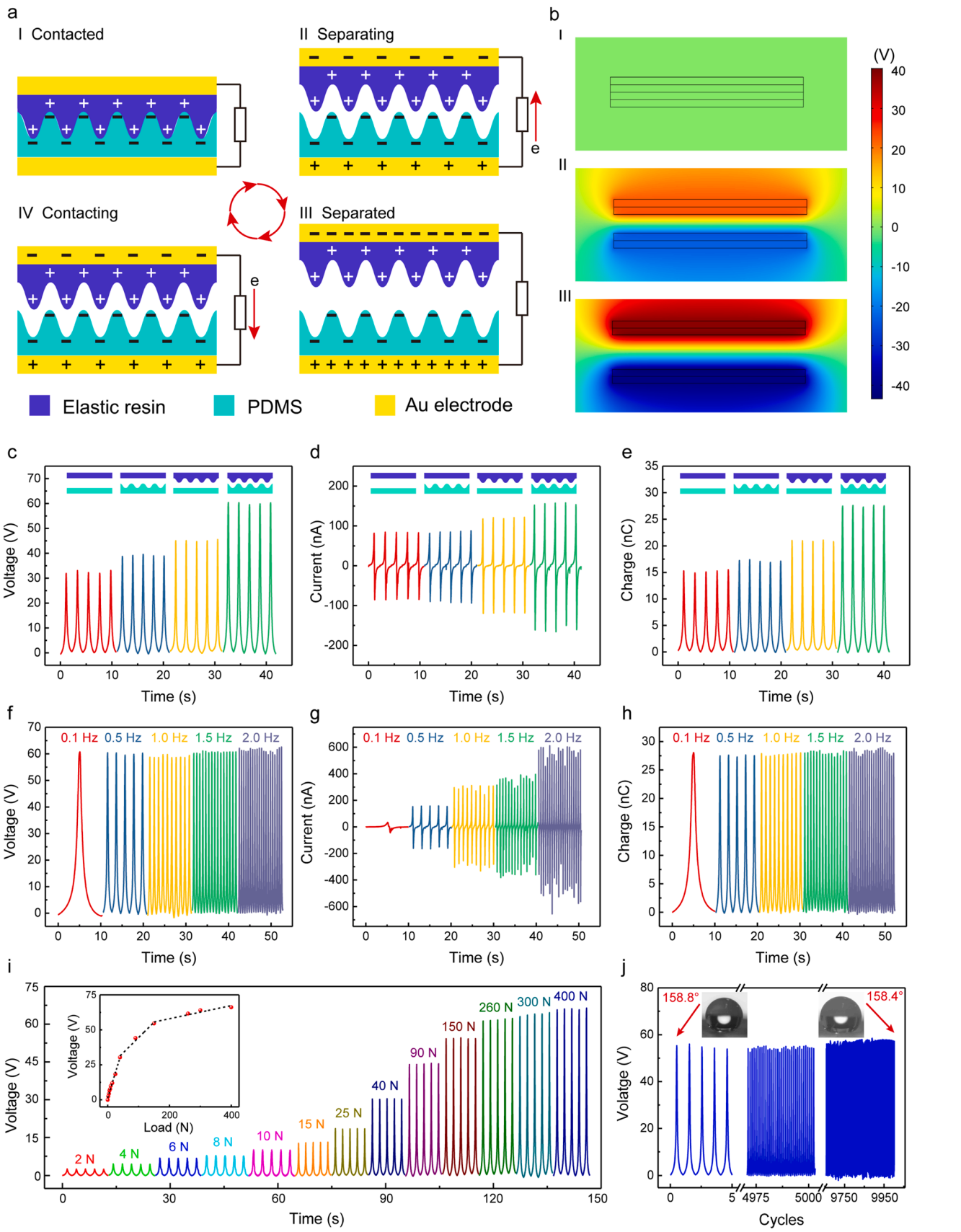

Fig. 3. (a) Working principle of the BSRW-TENG. (b) Simulated electric potential distribution on the triboelectric surfaces during contact and separation. (c) Open-circuit voltage, (d) short-circuit current and (e) transferred charges of TENGs with different triboelectric surfaces (flat resin & flat PDMS, flat resin & BH-PDMS, BH-resin & flat PDMS, and BH-resin & BH-PDMS). (f) Open-circuit voltage, (g) short-circuit current and (h) transferred charge of the BSRW-TENG under different working frequencies. (i) Open-circuit voltage of the BSRW-TENG under different loads. (j) Long-term stability of the BSRW-TENG.

formed between the two charged surfaces when they begin to separate, driving electrons flow from the bottom electrode to the top electrode due to electrostatic induction (state II). The flow of electrons last until the two surfaces are fully separated, which means a new electrostatic equilibrium is established (state III). Similarly, electrons would flow backwards from the top electrode to the bottom electrode when the two surfaces are contacting again (state IV) until an electrostatic equilibrium is established when they are fully in contact (state I). Finite element analysis (FEA) was conducted to simulate the electrical potential distribution during the three different states, as shown in Fig. 3**b**. The surface charge density applied in the simulation is 1e-5 C/m^2 approximately estimated from experimental results.

Micro/nanopatterning on the triboelectric surface is a widely applied method to increase the effective contact area, thus enhancing the output performance of TENGs. To investigate the impact of the bioinspired hierarchical micro/nanostructures on the electrical output of the BSRW-TENG, four kinds of TENG with different triboelectric surfaces, including flat resin and flat PDMS (flat-TENG), flat resin and BH-PDMS (BHP-TENG), BH-resin and flat PDMS (BHR-TENG), and BH-resin and BH-PDMS (BSRW-TENG), were fabricated and their corresponding electrical performances were tested. Unless otherwise specified, in the following tests the load applied, contact-separation distance and the frequency were set as 260 N, 5 cm and 0.5 Hz, respectively. Fig. 3**c-e** show the output open-circuit voltage, short-circuit current and transferred charges of the four TENGs. It can be seen that the output of the BSRW-TENG was twice as that of the flat-TENG, and about 1.5 times higher than that of the BHP-TENG and BHR-TENG. The BHR-TENG demonstrated a slightly higher output than the BHP-TENG, since the overall surface roughness of the BH-resin is slightly larger than the BH-PDMS. It is also interesting to investigate the effect of the nanostructures on the microtowers on the output performance of the TENG. Hence, a TENG with hydrophobic surfaces (H-TENG), which consists of the replicated PDMS without frame treatment and replicated Resin with least nanofolds and gullies (5 min UV curing) was fabricated and tested, as shown in Fig. S9. As can be seen, the formed nanostructures on the microtowers had an apparent enhancement on the output of the TENG. These results indicate that the bioinspired hierarchical micro/nanostructure morphology not only endowed the two triboelectric surfaces with self-cleaning property, but also enhanced the output performance of the BSRW-TENG.

The electrical output of the BSRW-TENG under various stimulation frequencies is demonstrated in Fig. 3**f-h**. It can be observed that the open-circuit voltage and transferred charges of the BSRW-TENG remained stable while the short-circuit current increased when the stimulation frequency increased. The reason is that the open-circuit voltage and transferred charges are only related to the contact area and contact-separation distance, while the short-circuit current increases with increasing contact-separation speed. The applied load has a decisive impact on the effective contact area between the two triboelectric surfaces, accordingly affecting the electric output. Fig. 3**i** shows the load response of the open-circuit voltage of the BSRW-TENG. The voltage increased gradually with the increase in the load, and then saturated at around 260 N. The micro/nanostructures on the triboelectric surfaces are expected to be anti-damageable in order to provide a continuous and stable enhancement on the output of TENGs. After 10,000 working cycles under such a large load (260 N), the micro/nanostructures on the BH-resin and BH-PDMS as well as their corresponding WCAs almost remained the same as those observed before testing, as demonstrated in Fig. S10. Such excellent stability in the micro/nanostructures and superhydrophobicity can be attributed to the strong elastic resilience of the resin and PDMS materials. Fig. 3**j** shows the output voltage of the BSRW-TENG and WCA of the BH-PDMS during the cyclic test, from which it can be seen that there is no obvious change in the output and WCA in 10,000 cycles, indicating the excellent long-term stability.

The output performance of TENGs is extremely easy to be affected and degraded due to surface contamination and high relative humidity (RH). Specifically, for wearable TENGs, sweat secreted by the human body is a main source of surface contamination and high RH. The RH change is understandable since the regional RH near the TENG must be increased due to the secretion of sweat. Besides, sweat would more or less flow and penetrate onto the triboelectric surfaces if there is no perfect encapsulation [17] which however would not only affect the wearable comfort but also the sensitivity of the TENG. Sweat could leave precipitated salt on the triboelectric surfaces after its evaporation, resulting in non-removable contaminations. To investigate the sweat-resistance ability of the BSRW-TENG, contamination-resistance and humidity-resistance properties of the BSRW-TENG were studied separately. Firstly, the influence of the surface contamination caused by sweat on the output performance of the BSRW-TENG was studied. Here, physiological saline (0.9%) was applied to simulate the sweat. Fig. 4**a** and **b** show different phases after the saline was dropped onto the bioinspired hierarchical surfaces and flat surfaces, which were tilted about 10°. As it can be seen, there were no saline droplets on the BH-resin and BH-PDMS because saline droplets slid away immediately due to the self-cleaning property of the bioinspired surfaces, while saline droplets stayed on the flat resin and flat PDMS all the time. As a result, the salt contained in the saline would be precipitated and left on the flat surfaces after saline droplets evaporated. Hereafter, the output performance of TENGs with different surfaces (flat-TENG, BHP-TENG, BHR-TENG and BSRW-TENG), on which the saline was dropped on and evaporated, were tested. As shown in Fig. 4**c**, the output of the flat-TENG degraded the worst, showing a 41% degradation. The BHP-TENG and BHR-TENG that possessed one self-cleaning surface demonstrated a much lower degradation (25.7% and 23.8%, respectively). The output of the BSRW-TENG in which both two triboelectric surfaces are self-cleaning almost remained the same. Then, the humidity-resistant abilities of the four TENGs were tested, as demonstrated in Fig. 4**d**. The output of the four TENGs all decreased when the RH increased from 10% to 80% (here, the output under room humidity (50% RH) was set as 100% for comparison). However, the influence of humidity on the output of the BSRW-TENG was observed to be quite small since the reduction was just 11%, while the flat-TENG decreased dramatically by 54%. The BHP-TENG and BHR-TENG demonstrated a similar reduction by about 23%. To reveal the superiority of the superhydrophobic surfaces over the hydrophobic surfaces, a TENG with only hydrophobic surfaces (H-TENG), consisting of the replicated PDMS without flame treatment and replicated resin with the least nanofolds and gullies (5 min UV curing), was also fabricated and tested under different humidity (Fig. S11). As can be seen, even the two triboelectric layers are nearly superhydrophobic, the humidity-resistant ability of the H-TENG is apparently lower than the BSRW-TENG. The above results depicted that the BSRW-TENG with two self-cleaning triboelectric surfaces featured excellent sweat-resistant ability.

The contamination-resistance and humidity-resistance of the BSRW-TENG was further verified under extreme harsh conditions, including severe surface contamination and water spraying. Carbon black powders that commonly adhere well on surfaces were applied to simulate the dust to fully contaminate the surfaces. A comparison of the self-cleaning ability of the flat surfaces and bioinspired hierarchical surfaces are demonstrated in Fig. S12a**, c** and **Video S3**, from which it can be seen that the dust on the BH-resin and the BH-PDMS can be easily removed by a syringe water jet. Fig. S12b and **d** also show optical images of the surfaces in different contamination phases, including original, contaminated, after water drop cleaning and 5 min ultrasonic cleaning. The BH-resin and the BH-PDMS were found to be almost completely cleaned and devoid of any carbon black residue just after water drop cleaning, while a significant amount of contamination residue still remained in the case of the flat surfaces even after ultrasonic cleaning.

Supplementary material related to this article can be found online at doi:10.1016/j.nanoen.2022.107018.

Fig. 4**e** and **f** show the output voltage of the flat-TENG and BSRW-

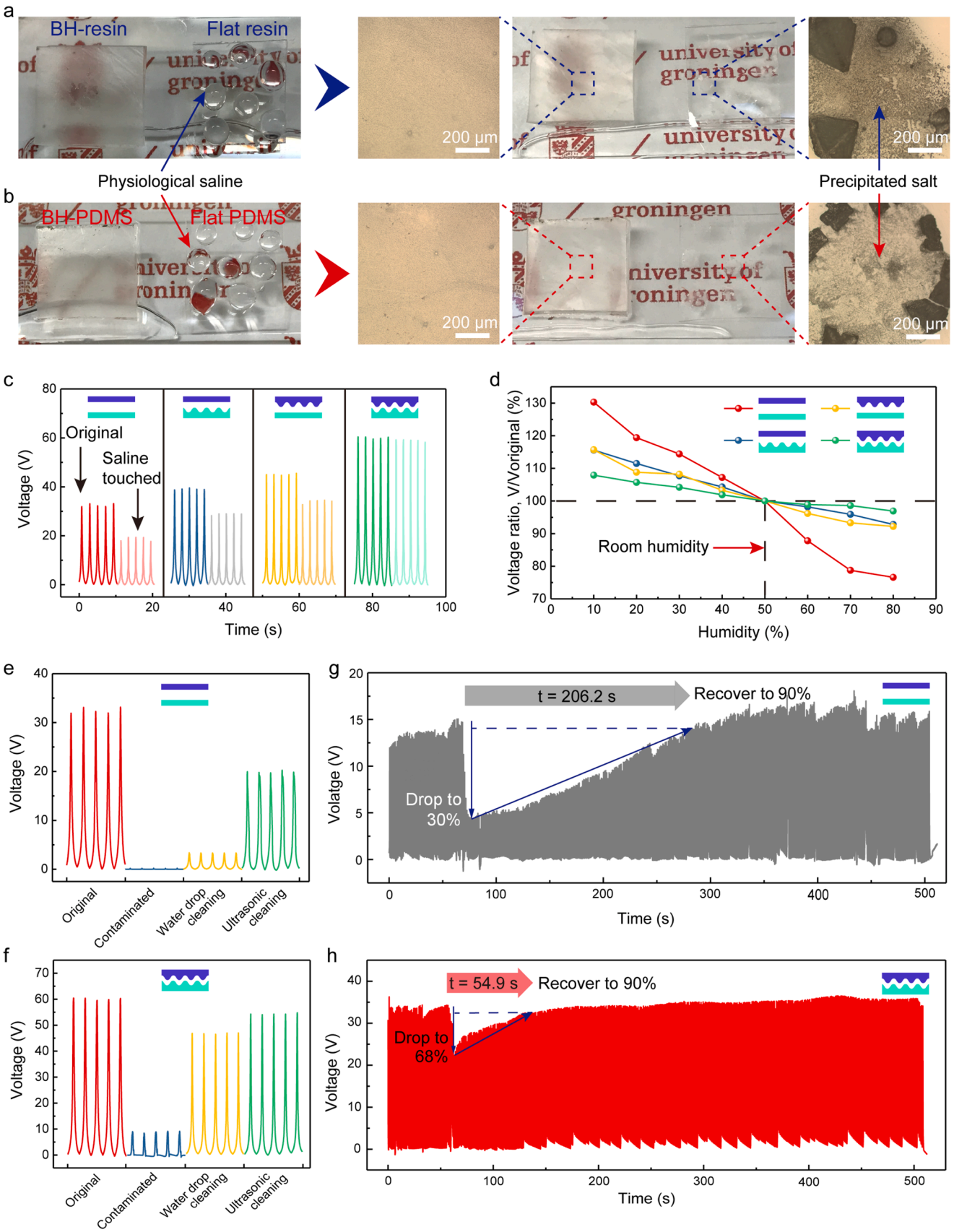

Fig. 4. (a and b) Demonstration of the sweat-resistant ability of (a) BH-resin and (b) BH-PDMS. (c) Outputs of TENGs with different triboelectric surfaces on which the saline was dropped on and evaporated. (d) Outputs of TENGs with different triboelectric surfaces under different relative humidities. (e and f) Outputs of TENGs with different triboelectric surfaces: (e) flat resin & flat PDMS and (f) BH-resin & BH-PDMS in different contamination phases (load = 260 N). (g and h) The recovery

of the output of TENGs with different triboelectric interfaces: (g) flat resin & flat PDMS and (h) BH-resin & BH-PDMS from 5 consecutive water spraying at the load of 40 N.

TENG in different contamination phases mentioned above, respectively. The outputs of the BHP-TENG and BHR-TENG are also shown in Fig. S13. After contamination, the most severe degradation of the output amongst the four TENGs was observed in the case of the flat-TENG, followed by the BHR-TENG and then the BHP-TENG and finally the BSRW-TENG, determined through drops in their output voltage from 33 V to 0.2 V, 44.5 V to 3 V, 39 V to 2.5 V, and 60 V to 9 V, respectively. The reason is that the dust on the superhydrophobic self-cleaning surfaces tends to fall away easily during the contact-separation test but adheres well on the flat surfaces. After cleaning using water droplets, the output of the BSRW-TENG recovered dramatically, increasing to 46.5 V that is 77.5% of the original output. In contrast, the flat-TENG, BHP-TENG and BHR-TENG only recovered to 3.3 V, 21 V and 25.5 V, which are 10%, 54% and 57% of their original output, respectively. Further ultrasonic cleaning enabled the output of the BSRW-TENG to increase to 54 V (90%) that is slightly higher than that of water drop cleaning, because the dust was almost already cleaned by water drop cleaning. For the flat surfaces, most dust can only be removed by ultrasonic cleaning, so the flat-TENG, BHP-TENG and BHR-TENG were able to recover to 20 V, 28.5 V and 37.5 V, respectively, after the ultrasonic cleaning.

Water spraying was applied to simulate the ultra-humid environment with water vapor, and the set-up is illustrated in Fig. S14. Here, the load was set to 40 N because water would be squeezed out immediately under a high load. Fig. 4**g** and **h** demonstrate the humidity-resistance and

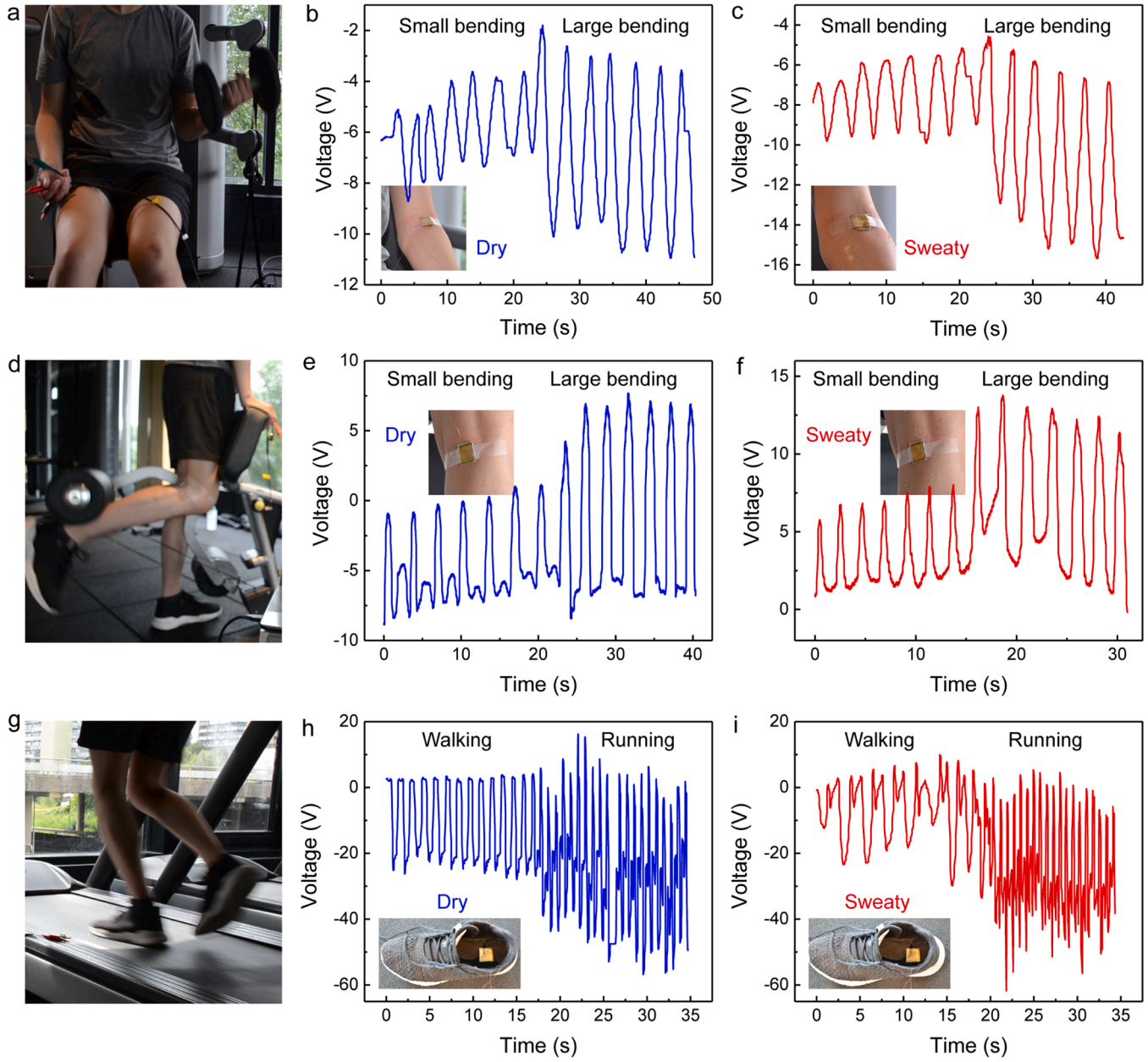

Fig. 5. (a) Photo of the BSRW-TENG attached on the elbow joint for dumbbell biceps curl monitoring. Bumbbell biceps curl monitoring results (b) before and (c) after sweating. d) Photo of the BSRW-TENG attached on the knee joint for leg curl monitoring. Leg curl monitoring results (e) before and (f) after sweating. g) Photo of the BSRW-TENG attached on the sole for running monitoring. Running monitoring results (h) before and (i) after sweating.

performance recoverability of the flat-TENG and BSRW-TENG after 5 consecutive water spraying. The outputs of the BHP-TENG and BHR-TENG are also demonstrated in Fig. S15. It can be seen that the output of all TENGs decreased instantaneously after water spraying and then gradually recovered to the original output. However, the more the self-cleaning triboelectric surfaces of the TENG, the lesser the output degradation and the faster the recovery. The output of the flat-TENG dropped the most to 30% of its original output and took the longest time (206.2 s) to recover to 90% of its original output. Equipped with a single self-cleaning surface, the performance of the BHP-TENG and BHR-TENG improved remarkably, dropping to 47% and 46% of their original outputs and then recovering to 90% of their original outputs in 82.3 s and 86.8 s, respectively. As expected, the BSRW-TENG demonstrated the best performance stability and recoverability, sustaining 68% of its original output. The recovery time for the BFSC-TENG is only 54.9 s, which is greatly shortened compared with the other TENGs. These results reflected the excellent performance stability and recoverability of the BSRW-TENG regardless of the severe dust contamination and/or ultra-humid water vapor, further illustrating the remarkable sweat-resistant ability of the BSRW-TENG. Compared to the previous works as listed in Table S1, our work realized excellent humidity-resistant and self-cleaning properties simultaneously on both two triboelectric layers through a simple, rapid and cost-effective fabrication method.

The BSRW-TENG featuring excellent sweat-resistant ability was then successfully applied to monitor movements during exercise and fitness. Here, dumbbell biceps curl, leg curl and running monitoring before and after body sweating are demonstrated as examples. As shown in Fig. 5**a** and **Video S4**, the BSRW-TENG was attached on the elbow joint to monitor the curling degree during dumbbell biceps curl. Fig. 5**b** and **c** show the monitoring results before and after sweating, respectively, from which one can see that the BSRW-TENG functioned stable in spite of the sweat secretion. The output of the BSRW-TENG increased when the bending degree increased as the contact area between two triboelectric layers increased, providing a judgement index on the completeness and effectiveness of the exercise motion. Similarly, the BSRW-TENG was attached on the knee joint to monitor the movement of leg curl (Fig. 5**d** and **Video S5**) with stable monitoring functionality before and after sweating (Fig. 5**e** and **f**). Interestingly, the output of the BSRW-TENG almost stayed the same but demonstrated an increasing inverted peak among the signal with the increased curling degree. This is because it was difficult for the BSRW-TENG to be conformally attached to the knee and the center of the BSRW-TENG tended to bend outward, resulting in the inverted peak. Nevertheless, the change of the inverted peak in the signal is found to be able to correctly indicate the curling degree of the knee. The BSRW-TENG was finally attached on a sole to monitor the running process (Fig. 5**g** and **Video S6**). As can be seen from the monitoring results shown in Fig. 5**h** and **i,** the BSRW-TENG can stably distinguish the walking and running statuses before and after sweaty. It is worth to note that various exercise parameters such as motion speed, frequency and even dynamic process can also be learned on demand from the monitored data, which can provide in-depth analysis and feedbacks for personal exercise monitoring and athlete's daily training analysis.

Supplementary material related to this article can be found online at doi:10.1016/j.nanoen.2022.107018.

3. Conclusion

In conclusion, we demonstrated a bioinspired sweat-resistant wearable triboelectric nanogenerator (BSRW-TENG) for exercise movement monitoring. Two bioinspired superhydrophobic and self-cleaning triboelectric layers (BH-resin and BH-PDMS) were realized by replicating the hierarchical micro/nanostructures from lotus leaf. TENGs with different triboelectric surfaces, including flat-TENG, BHP-TENG, BHR-TENG and BSRW-TENG, were fabricated and their corresponding electrical performances and sweat-resistance (contamination-resistant and humidity resistant) were tested and compared. The BSRW-TENG demonstrated a 2-fold increase in the output compared with the flat-TENG due to the hierarchical micro/nanostructures induced increase in the effective contact area. After saline dripped and evaporated on the triboelectric surfaces, the output of the BSRW-TENG remained the same while that of the flat-TENG decreased by 41% due to residual salt contamination. The BSRW-TENG also showed excellent humidity-resistant ability with a small reduction (11%) in the output when the RH increased from 10% to 80%, while the flat-TENG decreased 54%. The remarkable sweat-resistance was further verified under extreme harsh conditions, including full surface contamination and ultra-humid environment. Finally, various exercise movements, including dumbbell biceps curl, leg curl and running were successfully monitored by the BSRW-TENG with stable and sustainable performance before and after sweating. The proposed BSRW-TENG has huge potential for low-cost personal exercise monitoring and athletes' training analysis.

4. Experimental section

4.1. Fabrication of the bioinspired hierarchical resin (BH-resin)

A dried lotus leaf was cut into rectangular pieces (28 mm × 20 mm) that were then attached onto the bottom of a 3D-printed mold using double sided tape. PDMS (Sylgard 184 silicon elastomer) was prepared by mixing the base and curing agent in a weight ratio of 10:1 followed by degassing in a vacuum chamber until the bubbles disappeared. Thereafter, the uncured PDMS was poured into the mold to fully cover the lotus leaf, after which the curing process was conducted in an oven at 80 ℃ for 2 hrs. The cured PDMS was peeled off from the dried lotus leaf and served as the negative template. Elastic resin (Formlabs elastic 50 A resin) was cast on the PDMS negative templates and UV cured in a UV chamber at 60 ℃ for 5 min, 10 min, 15 min, 20 min and 25 min, respectively. Upon peeling, the BH-resin membranes were achieved successfully.

4.2. Fabrication of the bioinspired hierarchical PDMS (BH-PDMS)

A 10 nm-thick Cu intermediate sacrificial layer was deposited (Quorum Q150T ES) on the PDMS negative template before further casting PDMS to ensure that the two PDMS layers can be successfully demolded after the curing process. Following this, uncured PDMS was cast on top of the PDMS negative template and cured at 80 ℃ for 2 hrs. The unseparated PDMS block was then soaked in the $FeCl_3$ solution (1 mol/L) for 1 h to etch the Cu sacrificial interfacial layer. After taking the PDMS films out of the $FeCl_3$ solution, they were washed using ethanol and dried by air blowing. The PDMS replica was then peeled off from the PDMS negative template. Subsequent flame treatment for the PDMS replica was performed on a gas stove. The PDMS replica was held at a height of 20 mm (520 ± 10 ℃) from the post-reaction zone of the flame and moved back and forth along their length from one side to another side at a speed of 20 mm/s. After flame treated in 10 s, 20 s, 30 s, 40 s, and 50 s respectively, BH-PDMS membranes were fabricated.

4.3. Fabrication of the triboelectric nanogenerator

A 10 nm-thick Ti and 100 nm-thick Au layer was deposited on the backside of the PDMS and resin membranes (thickness: 300–400 μm) as electrodes through electron-beam evaporation (Temescal FC 2000). Copper wire was fixed on the Au electrode for electrical measurement. An ultra-thin PDMS layer (10 μm) was further spray coated on Au electrode to protect the electrode and connection. In detail, 5 g PDMS (base and curing agent) was mixed into 20 ml Tetrahydrofuran (THF, >99%, Sigma-Aldrich) solution and then magnetic stirred for 2 hrs to reduce the viscosity for the spray. After spraying, the samples were placed in the fume hood and cured at 80 ℃ for 24 hrs. At last, four TENGs with different interfaces, including flat resin and flat PDMS (flat-

TENG), flat resin and BH-PDMS (BHP-TENG), BH-resin and flat PDMS (BHR-TENG), and BH-resin and BH-PDMS (BSRW-TENG), were fabricated. For applications in monitoring exercise movements, double-sided sponge tape (thickness 1 mm) was applied as the spacer to ensure sufficient separation between the two triboelectric surfaces.

4.4. Characterization and measurement

The micro/nanostructures of the lotus leaf, PDMS negative template, BH-resin and BH-PDMS were analyzed using scanning electron microscopes (Tescan Lyra-3; Philips XL30 E-SEM). Optical images were analyzed using a digital microscope (Olympus digital microscope). The water contact angle on all the aforementioned surfaces was measured using an optical contact angle measurement instrument (Dataphysics 15EC). Finite element analysis (FEA) for electrical potential distribution simulation was conducted on COMSOL Multiphysics 5.2a. Electrostatics interface in the COMSOL AC/DC module and stationary study were applied to obtain the simulation results. Electrical measurements for the TENG were realized using an electrometer (Keithley 6514). The contact-separation motion between the two triboelectric surfaces was controlled in a fixed contact-separation distance (5 mm) with tunable velocity and frequency (MTS 810 Universal Testing Machine). The load was measured using pressure sensors (Chino Sensor, ZNLBM-5KG ($\leq$ 20 N); MTS 810 Universal Testing Machine ($>$ 20 N)). Carbon black (99 +%, Alfa Aesar) was used as artificial dust and a daily cosmetic spray bottle was used to generate water vapor. Physiological saline (0.9%) was synthesized by dissolving 0.9 g sodium chloride in 100 ml deionized water. Movement monitoring was carried out with assistance of a volunteer (the first author of this paper). The study was approved by the Research Ethics Review Committee (CETO) at the Faculty of Arts, University of Groningen and informed written consent was also obtained from the volunteer.

CRediT authorship contribution statement

Wenjian Li: Conceptualization, Methodology, Investigation, Data curation, Formal analysis, Visualization, Validation, Writing - Original Draft; **Liqiang Lu**: Data curation, Formal analysis, Visualization, Writing - Review & Editing; **Ajay Giri Prakash Kottapalli**: Resources, Validation, Writing – Review & Editing; **Yutao Pei**: Funding acquisition, Conceptualization, Supervision, Writing - Review & Editing.

Declaration of Competing Interest

The authors declare that they have no known competing financial interests or personal relationships that could have appeared to influence the work reported in this paper.

Acknowledgements

W.J.L. acknowledges China Scholarship Council, P. R. China for his Ph.D. scholarship (CSC, No. 201904910781). This work was partially supported by the University of Groningen's start-up grant awarded to A. G.P.K.

Appendix A. Supporting information

Supplementary data associated with this article can be found in the online version at doi:10.1016/j.nanoen.2022.107018.

References

[1] T. Vos, R.M. Barber, B. Bell, A. Bertozzi-Villa, S. Biryukov, I. Bolliger, F. Charlson, A. Davis, L. Degenhardt, D. Dicker, L. Duan, H. Erskine, V.L. Feigin, A.J. Ferrari, C. Fitzmaurice, T. Fleming, N. Graetz, C. Guinovart, J. Haagsma, G.M. Hansen, S. W. Hanson, K.R. Heuton, H. Higashi, N. Kassebaum, H. Kyu, E. Laurie, X. Liang, K. Lofgren, R. Lozano, M.F. MacIntyre, M. Moradi-Lakeh, M. Naghavi, G. Nguyen, S. Odell, K. Ortblad, D.A. Roberts, G.A. Roth, L. Sandar, P.T. Serina, J.D. Stanaway, C. Steiner, B. Thomas, S.E. Vollset, H. Whiteford, T.M. Wolock, P. Ye, M. Zhou, M. A. Āvila, G.M. Aasvang, C. Abbafati, A.A. Ozgoren, F. Abd-Allah, M. Aziz, S. F. Abera, V. Aboyans, J.P. Abraham, B. Abraham, I. Abubakar, L.J. Abu-Raddad, N. Abu-Rmeileh, T.C. Aburto, T. Achoki, I.N. Ackerman, A. Adelekan, Z. Ademi, A. K. Adou, J.C. Adsuar, J. Arnlov, E.E. Agardh, M.J. Al Khabouri, S.S. Alam, D. Alasfoor, M.I. Albittar, M.A. Alegretti, A.V. Aleman, Z.A. Alemu, R. Alfonso-Cristancho, S. Alhabib, R. Ali, F. Alla, P. Allebeck, P.J. Allen, M.A. AlMazroa, U. Alsharif, E. Alvarez, N. Alvis-Guzman, O. Ameli, H. Amini, W. Ammar, B. O. Anderson, H.R. Anderson, C. Antonio, P. Anwari, H. Apfel, V. Arsenijevic, A. Artaman, R.J. Asghar, R. Assadi, L.S. Atkins, C. Atkinson, A. Badawi, M.C. Bahit, T. Bakfalouni, K. Balakrishnan, S. Balalla, A. Banerjee, S.L. Barker-Collo, S. Barquera, L. Barregard, L.H. Barrero, S. Basu, A. Basu, A. Baxter, J. Beardsley, N. Bedi, E. Beghi, T. Bekele, M.L. Bell, C. Benjet, D.A. Bennett, I.M. Bensenor, H. Benzian, E. Bernabe, T.J. Beyene, N. Bhala, A. Bhalla, Z. Bhutta, K. Bienhoff, B. Bikbov, A.B. Abdulhak, J.D. Blore, F.M. Blyth, M.A. Bohensky, B.B. Basara, G. Borges, N.M. Bornstein, D. Bose, S. Boufous, R.R. Bourne, L.N. Boyers, M. Brainin, M. Brauer, C. Brayne, A. Brazinova, N. Breitborde, H. Brenner, A. Briggs, P.M. Brooks, J. Brown, T.S. Brugha, Global, regional, and national incidence, prevalence, and years lived with disability for 301 acute and chronic diseases and injuries in 188 countries, 1990–2013: a systematic analysis for the Global Burden of Disease Study 2013, Lancet 386 (2015) 743–800.
[2] R.B. Armstrong, G.L. Warren, J.A. Warren, Mechanisms of exercise-induced muscle fibre injury, Sports Med. 12 (1991) 184–207.
[3] A.N. Belcastro, L.D. Shewchuk, D.A. Raj, Exercise-induced muscle injury: a calpain hypothesis, Mol. Cell. Biochem 179 (1998) 135–145.
[4] M.J. Cima, Next-generation wearable electronics, Nat. Biotechnol. 32 (2014) 642–643.
[5] M. Bariya, H.Y.Y. Nyein, A. Javey, Wearable sweat sensors, Nat. Electro 1 (2018) 160–171.
[6] W. Gao, S. Emaminejad, H.Y.Y. Nyein, S. Challa, K. Chen, A. Peck, H.M. Fahad, H. Ota, H. Shiraki, D. Kiriya, D.H. Lien, G.A. Brooks, R.W. Davis, A. Javey, Fully integrated wearable sensor arrays for multiplexed in situ perspiration analysis, Nature 529 (2016) 509–514.
[7] T. Yang, X. Jiang, Y. Zhong, X. Zhao, S. Lin, J. Li, X. Li, J. Xu, Z. Li, H. Zhu, A Wearable and Highly Sensitive Graphene Strain Sensor for Precise Home-Based Pulse Wave Monitoring, ACS Sens. 2 (2017) 967–974.
[8] J. He, P. Xiao, W. Lu, J. Shi, L. Zhang, Y. Liang, C. Pan, S.-W. Kuo, T. Chen, A Universal high accuracy wearable pulse monitoring system via high sensitivity and large linearity graphene pressure sensor, Nano Energy 59 (2019) 422–433.
[9] G. Liu, S. Xu, Y. Liu, Y. Gao, T. Tong, Y. Qi, C. Zhang, Flexible Drug Release Device Powered by Triboelectric Nanogenerator, Adv. Funct. Mater. 30 (2020), 1909886.
[10] M. Amjadi, S. Sheykhansari, B.J. Nelson, M. Sitti, Recent Advances in Wearable Transdermal Delivery Systems, Adv. Mater. 30 (2018), 1704530.
[11] Y. Song, D. Mukasa, H. Zhang, W. Gao, Self-Powered Wearable Biosensors, Acc. Mater. Res. 2 (2021) 184–197.
[12] F.-R. Fan, Z.-Q. Tian, Z. Lin Wang, Flexible triboelectric generator, Nano Energy 1 (2012) 328–334.
[13] Y. Song, N. Wang, C. Hu, Z.L. Wang, Y. Yang, Soft triboelectric nanogenerators for mechanical energy scavenging and self-powered sensors, Nano Energy 84 (2021), 105919.
[14] H. Wang, M. Han, Y. Song, H. Zhang, Design, manufacturing and applications of wearable triboelectric nanogenerators, Nano Energy 81 (2021), 105627.
[15] W. He, X. Fu, D. Zhang, Q. Zhang, K. Zhuo, Z. Yuan, R. Ma, Recent progress of flexible/wearable self-charging power units based on triboelectric nanogenerators, Nano Energy 84 (2021), 105880.
[16] H. Chen, Y. Song, X. Cheng, H. Zhang, Self-powered electronic skin based on the triboelectric generator, Nano Energy 56 (2019) 252–268.
[17] Y. Zou, V. Raveendran, J. Chen, Wearable triboelectric nanogenerators for biomechanical energy harvesting, Nano Energy 77 (2020), 105303.
[18] Y. Lee, S.H. Cha, Y.W. Kim, D. Choi, J.Y. Sun, Transparent and attachable ionic communicators based on self-cleanable triboelectric nanogenerators, Nat. Commun. 9 (2018) 1804.
[19] J. Shen, Z. Li, J. Yu, B. Ding, Humidity-resisting triboelectric nanogenerator for high performance biomechanical energy harvesting, Nano Energy 40 (2017) 282–288.
[20] Q. Zheng, Y. Jin, Z. Liu, H. Ouyang, H. Li, B. Shi, W. Jiang, H. Zhang, Z. Li, Z. L. Wang, Robust Multilayered Encapsulation for High-Performance Triboelectric Nanogenerator in Harsh Environment, ACS Appl. Mater. Interfaces 8 (2016) 26697–26703.
[21] B. Jiang, Y. Long, X. Pu, W. Hu, Z.L. Wang, A stretchable, harsh condition-resistant and ambient-stable hydrogel and its applications in triboelectric nanogenerator, Nano Energy 86 (2021), 106086.
[22] S. Adonijah Graham, B. Dudem, H. Patnam, A.R. Mule, J.S. Yu, Integrated Design of Highly Porous Cellulose-Loaded Polymer-Based Triboelectric Films toward Flexible, Humidity-Resistant, and Sustainable Mechanical Energy Harvesters, ACS Energy Lett. 5 (2020) 2140–2148.
[23] M.-O. Kim, S. Pyo, G. Song, W. Kim, Y. Oh, C. Park, C. Park, J. Kim, Humidity-Resistant, Fabric-Based, Wearable Triboelectric Energy Harvester by Treatment of Hydrophobic Self-Assembled Monolayers, Adv. Mater. Technol. 3 (2018), 1800048.
[24] Y.-T. Jao, P.-K. Yang, C.-M. Chiu, Y.-J. Lin, S.-W. Chen, D. Choi, Z.-H. Lin, A textile-based triboelectric nanogenerator with humidity-resistant output characteristic and its applications in self-powered healthcare sensors, Nano Energy 50 (2018) 513–520.

[25] C.M. González-Henríquez, F.E. Rodríguez-Umanzor, D. Guzmán, M.A. Sarabia-Vallejos, J. Rodríguez-Hernández, Formation of responsive hierarchical wrinkled patterns on hydrogel films via multi-step methodology, Polymer 179 (2019), 121662.
[26] S.K. Basu, L.E. Scriven, L.F. Francis, A.V. McCormick, Mechanism of wrinkle formation in curing coatings, Prog. Org. Coat. 53 (2005) 1–16.
[27] G. Li, D. He, Y. Lin, Z. Chen, Y. Liu, X. Peng, Fabrication of biomimetic superhydrophobic surfaces by a simple flame treatment method, Polym. Adv. Technol. 27 (2016) 1438–1445.
[28] N. Atthi, W. Sripumkhai, P. Pattamang, O. Thongsook, R. Meananeatra, P. Saengdee, A. Srihapat, J. Supadech, T. Janseng, A. Maneesong, N. Kongto, A. Rodchanarowan, N. Klunngien, W. Jeamsaksiri, Superhydrophobic and superoleophobic properties enhancement on PDMS micro-structure using simple flame treatment method, Microelectron. Eng. 230 (2020), 111362.

Mr. Wenjian Li received his B.E. degree in Mechanical Engineering from China University of Geosciences, Wuhan in 2016 and M.S. degree in Nanoscience and Technology from Beijing Institute of Nanoenergy and Nanosystems, Chinese Academy of Sciences in 2019. Now, he is a Ph.D. candidate at the University of Groningen, The Netherlands. His research interests mainly focus on self-powered sensors and systems, triboelectric nanogenerators, bionics, and self-powered applications for Internet of things.

Dr. Liqiang Lu received his Ph.D. from the University of Groningen in 2018. He is now a postdoctoral researcher at the University of Groningen. His research interests mainly focus on tuning the electrochemical properties and performances of energy storage materials in order to develop advanced electrochemical energy storage devices with high energy density, low-cost and long lifespan.

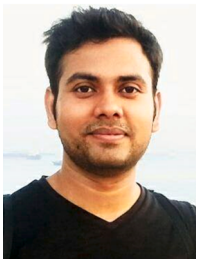

Dr. Ajay Kottapalli is an assistant professor in the Department of Advanced Production Engineering at University of Groningen. In 2013, he received his Ph.D. degree from Nanyang Technological University. During 2014–2015, he was a Postdoctoral Associate at Singapore-MIT Alliance for Research and Technology (SMART) and in 2016 he became a Principal Research Scientist at SMART. He is also currently a Research Affiliate with the MIT Sea Grant at MIT. In 2018, he was awarded the top-10 innovators under 35 in Asia-Pacific by MIT Technology Review. His research interests mainly include biomimetic/bio-inspired MEMS/NEMS, nanoelectronics, TENG and PENGs, and biomedical sensors.

Prof. Yutao Pei is a professor in the Department of Advanced Production Engineering at the University of Groningen. He received his Ph.D. degree in Exploration Engineering from China University of Geosciences, in 1992. During 1993–1994, he was a postdoctoral fellow at Harbin Institute of Technology. In 1995, he became an associate professor at Beijing University of Technology. Since 1998, he joined the Netherlands Institute for Metals Research that was transformed in 2008 into the Materials Innovation Institute M2i. His current research interests mainly include nanostructured materials for energy storage, additive manufacturing, laser materials processing, surface engineering and coating technology.